CFD Simulation of Melting and Solidification of PCM in Thermal Energy Storage Systems of Different Geometry

2015 J. Phys.: Conf. Ser. 655 012051

(http://iopscience.iop.org/1742-6596/655/1/012051)

Journal of Physics: Conference Series **655** (2015) 012051 doi:10.1088/1742-6596/655/1/012051

CFD Simulation of Melting and Solidification of PCM in Thermal Energy Storage Systems of Different Geometry

S Arena, G Cau, C Palomba*
Dept. of Mechanical, Chemical and Materials Engineering, University of Cagliari, Via Marengo 2, 09123 - Cagliari, Italy

* In memory of Chiara, dear friend and estimated researcher, who left us on May 15.

E-mail: simonearena@unica.it

Abstract. At the Department of Mechanical, Chemical and Materials Engineering of the University of Cagliari an experimental and numerical research project has begun with the aim of developing highly efficient thermal energy storage (TES) systems using phase change materials (PCM) of particular interest in concentrating small-medium scale solar power (CSP) applications. The present work aims to simulate the melting and solidification processes in containing boxes and heat transfer devices of different geometrical features which may constitute the elementary cell of a more complex TES system.

Two-dimensional axisymmetric numerical models, developed with COMSOL Multiphysics are considered and used to simulate TES, heat conduction and natural convection. The models are used to determine the temperature profile inside the PCM to identify which configurations are capable of enhancing thermal response between a solid wall and a PCM. The results obtained will be used for comparison with experimental data acquired from a pilot plant under construction in the DIMCM laboratories. At the current stage the laboratory is being brought to completion.

1. Introduction

The growing worldwide energy demand for human activities, mainly based, also in perspective, on fossil fuels, raises the question of sustainability. In particular, as regards the atmospheric concentration of CO_2, renewable energy sources together with power generation efficiency and end-use fuel and electricity efficiency are going to play a fundamental role and will contribute for about 60% to the overall reduction of CO_2 emissions. As is know, renewable energy sources such as solar and wind energy in particular, are not only characterized by discontinuous availability but are also affected by random variations due to local weather conditions. To expand their use, some form of energy storage must be foreseen to permit the deferred use of excess energy produced during periods of high availability or low demand. The development of phase change materials (PCM) for thermal energy storage (TES) is framed in the course of action in which thermal energy at medium-high temperature from, as an example, solar concentration fields or industrial processes, needs to be stored for optimum management. The advantage of this type of storage is that of maintaining a constant temperature of the working fluid preserving its potential to produce work in power generation systems in particular.

However, while it is relatively simple to size the amount of a given material required to store a definite amount of energy, it is more complex to design a phase changing heat exchanger that allows

performance of the heat transfer process between PCM and HTF in an efficient way. The heat transfer will influence the time required to store and release the thermal energy and it is therefore a fundamental design parameter when a PCM-TES must interact dynamically with other equipment such as, for example, a solar field and a thermal engine. Poor heat transfer during the charging period will lower solar field efficiency with high re-entry temperatures of the heat transfer fluid. Similar considerations may be drawn for the discharging period when the required thermal power must be supplied, for instance, to a thermal engine.

A number of experimental and theoretical studies on the transient thermal behaviour and performance of a thermal energy storage device during both charging and discharging processes have been conducted by several investigators. Adine and Karma [1] , Akgun et al. [2] and Gil et al.[3] investigated the performance of a shell and tube thermal energy storage device. Gil et al. [4][5][6][7], Solè et al.[8], Medrano et al. [9] studied different types of materials for applications in the field of concentrated solar energy systems at medium temperature. The results show that the selection of operating conditions and geometric parameters depends on the required heat transfer rate and the time in which the energy has to be stored or released. The main disadvantages of PCMs is low thermal conductivity which requires a long time for the melting and solidification processes. Several common techniques have been employed to enhance the heat transfer rate of PCMs. Choi and Kim [10] and Castell et al. [11] used finned tubes, Velraj et al. [12] used rings and bubble agitation, Melhing et al.[13] proposed a graphite compound-material, Agyenim et al. [14] and Al-Abidi et al. [15] proposed a triplex tube heat exchanger (TTHX). This system is composed of three tubes: the heat transfer fluid flows in the inner and outer tubes while the PCM is placed in the middle tube. This configuration increases the heat transfer area, thus improving heat transfer efficiency with respect to that of the double pipe heat exchanger.

The purpose of this analysis is focused on the development of thermal energy storage systems, to be used as back-up devices during transient operations of small and medium scale concentrated solar plants (CSP). Real applications of LHTES for the temperature range chosen (150-220 °C) are typically used in solar technologies associated with Organic Rankine Cycle (ORC) (e.g. REELCOOP EU/FP7 project). In the same temperature range, PCM materials are also used in various types of industrial applications such as in solar cooling systems with absorption chiller [3], related to fuel cell PAFC or heat recovery in metal hydrides hydrogen storage systems.

In the present work, three different geometrical configurations of heat exchangers were investigated numerically. The first configuration is a simple double-pipe, the second is a TTHX and the third is a TTHX with circular fins. The effects of natural convection were considered and the different distributions of heat transfer in the three cases were studied to evaluate the effects of charging and discharging processes on heat transfer coefficients and execution.

2. Material and method

2.1. Phase change material selection

The choice of PCM was mainly made on the basis of a melting temperature range suitable for implementation of a TES system in small-size concentrating solar plants. In this case, the system operates with an upper temperature of 200 °C, which represents the maximum temperature of the HTF leaving the solar collectors. The latent heat is also a significant choice parameter, since on it depends the amount of energy storable per unit mass of PCM. The final choice must also take into consideration other relevant parameter such as chemical properties, thermal expansion and safety.

For the present study, D-Mannitol was selected from among different PCM candidates after a literature review [4][5][9][13][16][17] since it has a phase change temperature range between 164 and 170 °C and a melting enthalpy of 316 kJ/kg [16]. D-Mannitol is classified as a sugar alcohol, molecular formula $C_6H_{14}O_6$: it is derived from a sugar (mannose) by reduction. The properties of D-Mannitol are shown in Table 1. Thermophysical properties of the liquid phase were obtained from

other materials belonging to the same family and with similar transition temperatures with an estimated uncertainty of about 10%. Although widely used in other fields (pharmaceuticals, food industry etc.), only in recent years has this kind of materials been studied and used for thermal energy storage. As concerns latent heat, a value of 316 kJ/kg was found in literature [16], obtained for the pure substance and under controlled conditions, but several tests with the DSC [6][18][19][20][20]. detected that this value depends strongly on three important factors, namely purity, cooling/heating rate and air contact. For these reasons, a more "realistic" value of 234 kJ/kg was used in this work.

Table 1. Properties of D-Mannitol.

	Solid	Liquid
Density (kg/m^3)	1520 (20 °C)	1382
Specific heat (kJ/kgK)	1.320 (20 °C) [a]	1.452
Thermal conductivity (W/mK)	0.279 [b]	0.307
Phase change temperature	167°C	
Range of phase transition temperature	±3°C	
Latent heat	234 kJ/kg [c]	

[a] NIST web page (National Institute of Standards and Technology).
[b] Thermal Energy Storage Systems for Solar Cookers, www.ukessays.com
[c] value obtained as the average of the experimental results found in literature [6][18][19][20][21].

2.2. Design of the PCM storage systems

Three cases with different geometrical configurations were considered in characterizing the TES system. Case 1 (Fig. 1a) is based on the configuration of the double-tube heat exchanger, where the outer tube is filled with PCM while the heat transfer fluid (HTF) flows in the inner tube. Case 2 (Fig. 1b) is based on a triplex heat exchanger. It is composed of three tubes: the HTF flows in the outer and inner tubes, while the PCM is placed between them. Case 3 (Fig. 1c) is a triplex with six circular fins. “Syltherm 800” was selected as the heat transfer fluid, as it is the HTF used in the experimental facility under construction.

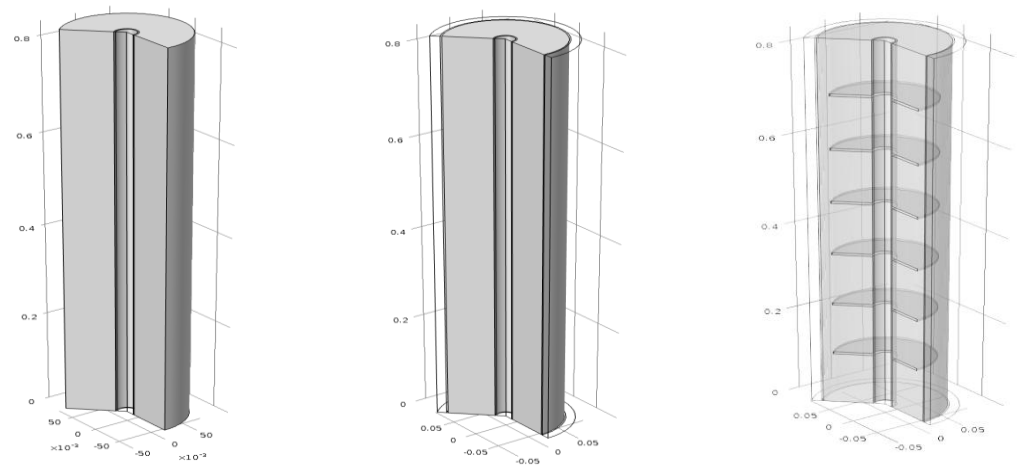

(a) Case 1 - Double tube (b) Case 2 - Triplex (c) Case 3 - Triplex with fins

Figure 1. Geometrical configuration of the three TES systems.

The design of the storage systems is based on the LMTD method and was performed by means of a computer code developed in Matlab environment. The geometrical characteristics of the three TESs are shown in Table 2. The value of HTF mass flow rate was selected as 0.052 kg/s for all three cases analyzed for both charge and discharge phases. The HTF temperature at the inlet of the accumulator was chosen as 180 °C and 100 °C for charge and discharge respectively. The HTF flows from top to bottom during both charge and discharge phases. The PCM mass for Cases 1 and 2 was 23.4 kg, while for Case 3, owing to the space occupied by the fins, the value was slightly lower, 22.8 kg, allowing a thermal energy storage of about 3 kWh.

Table 2. Geometrical characteristics of the storage system

	Case 1	Case 2	Case 3
Heat transfer surface [m^2]	0.077	0.568	0.73
Internal Diameter inner tube [m]	0.0254 (1")	0.0254 (1")	0.0254 (1")
Outside Diameter tube PCM [m]	0.127 (5")	0.127 (5")	0.127 (5")
Outside Diameter outer tube HTF [m]	-	0.2218	0.2218
Length [m]	0.83	0.83	0.83
Number of fins	-	-	6
Fin Length [m]	-	-	0.05
Fin thickness [m]	-	-	0.005
Tube thickness (Steel) [m]	0.002	0.002	0.002

2.3. Mathematical model of the PCM thermal energy storage system

A 2D axisymmetric numerical model was developed with the COMSOL Multiphysics 5.0 platform to simulate the transient and energy behaviour of the entire PCM-TES system during the phase change processes. Three different "physics", described below, were used to create the model [22]. The first and the third physics, "Fluid Flow", were used to simulate the behaviour of the HTF and the liquid PCM, the second, "Heat Transfer", was used to simulate the heat transfer process between the HTF and the PCM; it is composed of three sub-modules: heat transfer by convection, by conduction and phase change heat transfer.

2.3.1. Fluid Flow (HTF)

To simulate the dynamic behaviour of the HTF flowing inside the inner tube (Case 1) and inside the inner and the outer tubes (Case 2-3), the continuity equation (1) and the momentum equation (2) were used. The flow is considered laminar and incompressible and the effect of gravity is negligible (F=0).

$$\frac{\partial \rho}{\partial t} + \nabla \cdot (\rho u) = 0 \tag{1}$$

$$\frac{\partial \rho u}{\partial t} - \nabla \cdot \left[\mu\left(\nabla \mathrm{u} + (\nabla \mathrm{u})^{\mathrm{T}}\right)\right] + \rho(u \cdot \nabla)u + \nabla p = F \tag{2}$$

In equations (1) and (2), ρ and μ are the density and the dynamic viscosity of the HTF respectively, u is the velocity vector and p is the pressure.

2.3.2. Heat Transfer in Fluid
Heat transfer from the HTF to the wall of the steel tube takes place by convection. The energy equation (3) was solved using the velocities found from the solution of Eqs. (1) and (2). In equation (3) C_p and k are respectively the specific heat and the thermal conductivity of the material.

$$\rho C_p \frac{\partial T}{\partial t} + \rho C_p u \cdot \nabla T = \nabla \cdot (k \nabla T) \tag{3}$$

2.3.3. Heat Transfer in Solid
Heat transfer from the wall of the steel tube to the PCM takes place by conduction. The energy equation (4) for this case is reported below:

$$\rho C_p \frac{\partial T}{\partial t} = \nabla \cdot (k \nabla T) \tag{4}$$

2.3.4. Heat Transfer with Phase Change
The energy equation (5), in accordance with the apparent heat capacity formulation (6), was used to obtain the temperature field. This method assumes that the transformation occurs in a temperature interval between $(T_m - \Delta T_m/2)$ and $(T_m + \Delta T_m/2)$ where the material phase is modelled by a smoothed function α, representing the fraction of phase that generates during transition. The value of this function is equal to 0 before $(T_m - \Delta T_m/2)$ and to 1 after $(T_m + \Delta T_m/2)$. The equivalent heat conductivity and density are given by equations (7) and (8) in which the parameter $\theta = (1 - \alpha)$ is introduced.

$$\rho C_p \frac{\partial T}{\partial t} + \rho C_p u \cdot \nabla T = \nabla \cdot (k \nabla T) \tag{5}$$

$$C_p = \theta C_{p,phase1} + (1 - \theta) C_{p,phase2} + L \frac{\partial \alpha}{\partial T} \tag{6}$$

$$k = \theta k_{phase1} + (1 - \theta) k_{phase2} \tag{7}$$

$$\rho = \frac{\theta \rho_{phase1} C_{p,phase1} + (1 - \theta) \rho_{phase2} C_{p,phase2}}{\theta C_{p,phase1} + (1 - \theta) C_{p,phase2}} \tag{8}$$

2.3.5. Fluid Flow (liquid PCM)
The continuity and momentum equations (1) and (2) were used to simulate the behaviour of the PCM in liquid phase. To simulate the buoyancy force giving rise to natural convection, a volume force was added. The Boussinesq approximation was introduced to consider these buoyancy forces, according to Eq. (9). In this case ρ, μ and β are respectively the density, the dynamic viscosity and the thermal expansion coefficient of the liquid PCM, g is the gravitational constant and T_m is the melting temperature. The flow is considered laminar and incompressible.

$$F_b = g \rho \beta (T - T_m) \tag{9}$$

In this method, the entire PCM was treated as a liquid, even when its temperature was lower than its melting point. A modified viscosity was used to force this liquid to behave as a solid when required. A step function, continuous second derivative centred at about T_m, was introduced to define the modified viscosity: the value of this step function was 10^6 for the solid PCM and the actual value of μ for the

liquid PCM. This approach forces the Navier-Stokes equation to calculate the velocity everywhere, even when the PCM is a solid. This significantly increases the number of calculations and the possibility that the solver will diverge during the simulation. A second volume force, defined by Eq. (10), was added to the momentum equation to calculate velocities equal to zero in the solid phase of PCM.

$$F_v = -A(T) \cdot \mathrm{u} \tag{10}$$

In this equation a step function $A(T)$ was introduced: its value was 10^8 for the solid PCM and zero for the liquid PCM. The role of F_v is to dominate every other force terms in the momentum equation (2) when the PCM is solid, thus improving the time of calculation and effectively forcing a trivial solution of $u = 0$ in the solid. This method is mathematically better defined and allows a reduction of the number of iterations performed by the solver.

3. Results and discussion

In this paragraph the simulation results of the three cases considered are presented. Figures 2 and 3 show the temperature evolution of the PCM evaluated at the bottom of the accumulator (in proximity of the HTF outlet), in function of time during charge (Fig. 2) and discharge (Fig. 3).

In charging mode, the process started from a homogeneous initial state of the entire system (PCM, tubes, and HTF). At the beginning, the entire PCM system was at the set temperature of 100 °C, with an inlet temperature of the HTF of 180 °C. In this condition the heat transfer inside the solid PCM was governed by conduction. Then, when the temperature range of phase transition was reached, the melting process began. During the phase transition both conduction and natural convection in liquid phase occurred. At the end of the transition process, the PCM was in the liquid phase. In this condition, the heat transfer inside the liquid PCM was governed by convection.

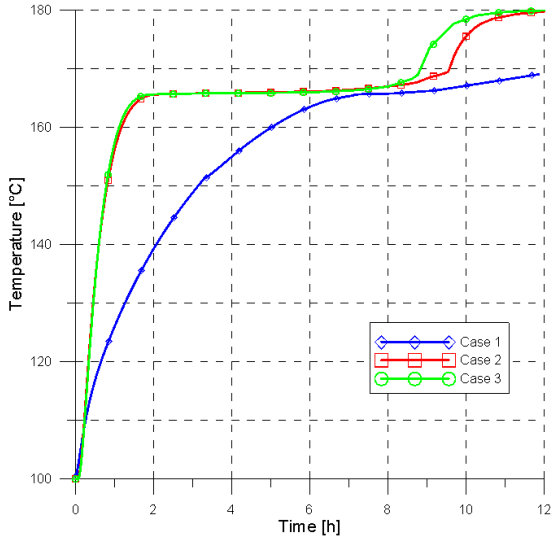

Figure 2. PCM temperature profile, charge.

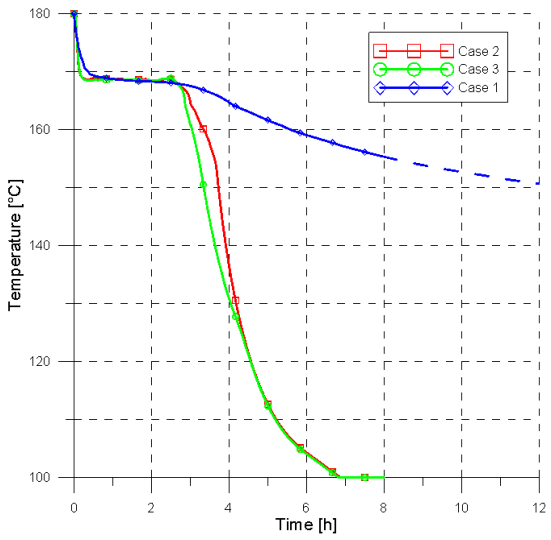

Figure 3. PCM temperature profile, discharge

The discharging process was performed analogously. Initially, the entire PCM system was at the set temperature of 180 °C, with an inlet temperature of the HTF of 100 °C. The time of the charge and discharge processes was imposed as 12 and 8 hours respectively. In the charge phase the transition process finished after approximately 10 hours, while in the discharge phase the complete transition was reached in about 3.5 hours.

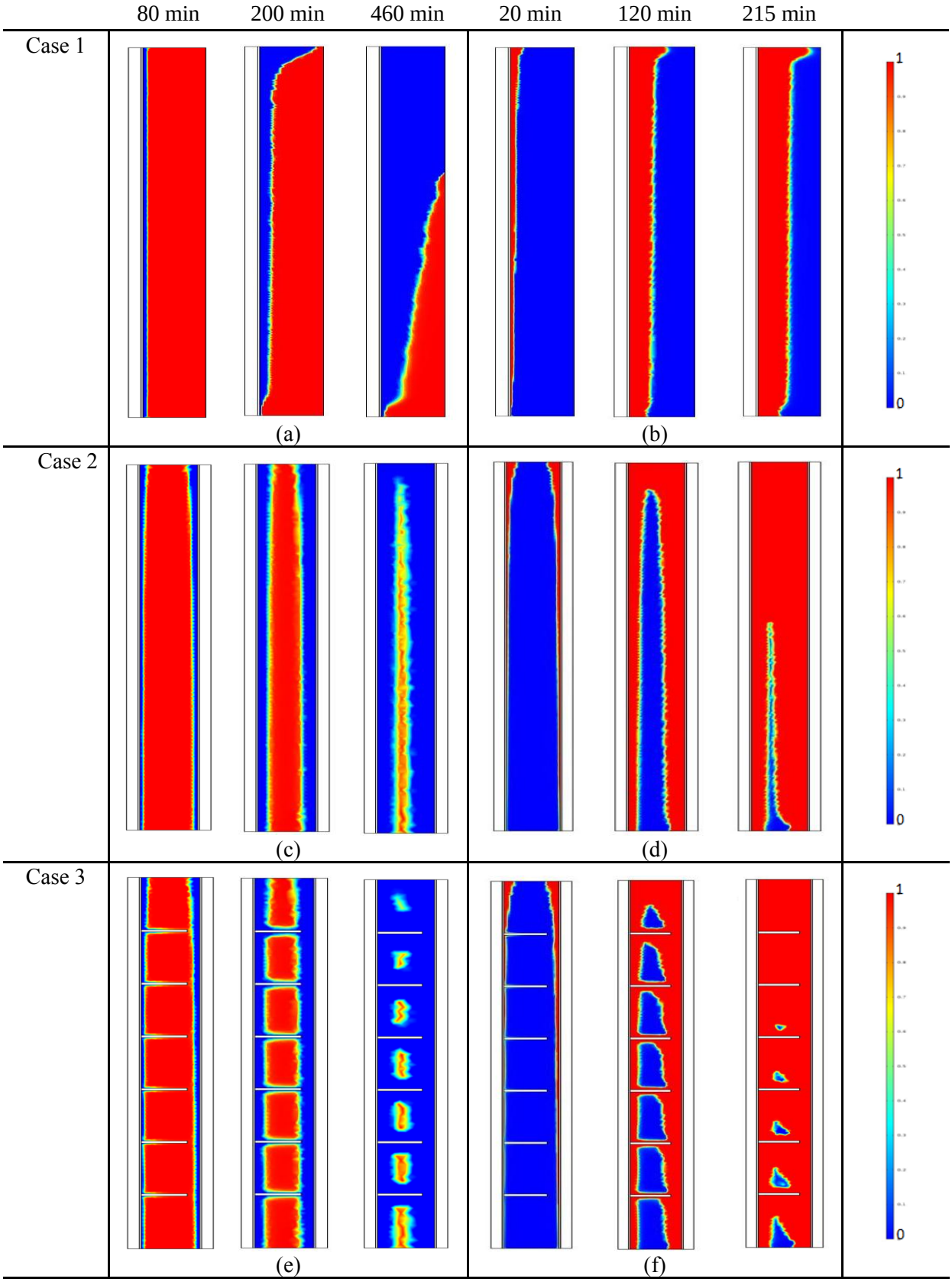

Figure 4. Phase evolution of PCM during charge and discharge process

As expected, the melting process took longer than solidification owing to the lower temperature difference between PCM during transition and HTF at the accumulator inlet, approximately 15 °C during charge and 70 °C during discharge. As expected, Case 3 presents the lowest time of charge and discharge, owing to the enhanced heat transfer surface which allows the exchange of higher and more uniform thermal power with respect to the other cases. Figs. (2-3) illustrate that neither in the charging nor in the discharging phase does Case 1 reach the equilibrium condition for melting/solidification respectively. In fact, after 12 hours of charge and 8 hours of discharge, the PCM shows a lower value of temperature than the HTF. Therefore, in this case the charge and the discharge processes are much slower than in the other two cases. The dashed line refers to the condition where Case 1 continues for 12 hours as for the charge phase.

Fig. (4) shows the phase change evolution of the PCM during charge (a,c,e) and discharge (b,d,f) processes. The figures show a cross section of the TES in which the inner tube is on the left side while the wall (Case 1) or the outer tube (Case 2-3) are on the right side. The red area represents the solid phase of the PCM material, the blue area represents the liquid phase. It can be observed that the solid-liquid interface moves in different time steps depending on the different geometrical configurations.

It is evident that Case 2 and Case 3 have a more homogeneous heat transfer rate with respect to Case 1. After 80 min, the solid-liquid interface starts to form at the top of the TES, where the HTF enters and along the entire length of the inner tube (Case 1) and of the inner and outer tubes (Cases 2-3). Fig. 4e shows that for this time step a film of liquid PCM starts to form also around the fins. After 200 min it is possible to note the different characteristics of the solid-liquid interface for the three cases on account of their different configurations. In Case 1 the solid-liquid interface moves parallel and radially from the centre to the peripheral wall. On the top of the TES device it is possible to observe a larger area of liquid PCM, owing to the proximity of the HTF inlet, while a smaller area appears on the bottom. In Case 2 the interface assumes a kind of parabolic shape (Fig 4c,d), while in Case 3 various cells with liquid PCM form during the process (Fig. 4e,f). In Case 1, after 460 min of charge, a large area of solid material can still be seen (Fig. 4a) while, in Case 2 only a narrow portion in the mid part of TES device remains in solid phase (Fig. 4c). For Case 3, the solid PCM forms small spots into the cells between the fins (Fig. 4e). A similar behaviour can be seen for the discharge phase, but the time to reach complete melting is lower with respect to the charge phase.

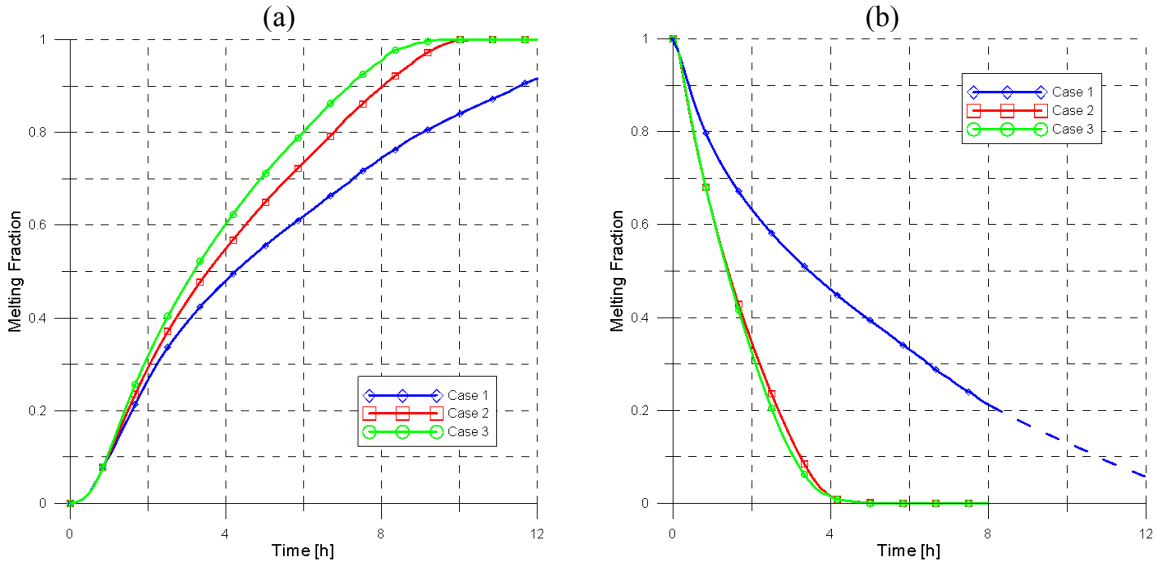

Figure 5. Melting Fraction for charge (a) and discharge (b) processes.

Figure (5) presents the PCM melted fraction versus time for the charge (a) and discharge (b) processes. This parameter is defined as the volume of PCM in liquid phase divided by the total volume

occupied by the PCM. By definition, the melted fraction is 0 at the beginning of the charge process and 1 at the beginning of the discharge process. As mentioned, the lowest melting and solidification time was obtained for Case 3. Moreover, it is evident that Case 1 does not reach complete melting and solidification after 12 and 8 hours of charge and discharge respectively. The dashed line again refers to the condition where Case 1 continues for 12 hours as for the charge phase. For Cases 2-3, in the charge phase the melting fraction is equal to 1 after about 9-10 hours and the whole PCM is in the liquid phase. At the same time, for Case 1 the melted fraction is between 0,80-0,84. In the discharge phase, after about 5 hours the melting process is complete for Cases 2-3, while at the same time the value of the melting fraction is about 0.40 for Case 1.

4. Conclusions

Three different geometrical configuration of a TES system were studied to identify the best solution as regards thermal energy storage with PCM materials. A double tube (Case 1), a triplex (Case 2) and a triplex with circular fins (Case 3) were analyzed to evaluate temperature and phase distribution in both charge and discharge phases. It was found that the different configurations of the three systems considered had a strong impact on the performance of the phase change process.

In Case 1 the solid-liquid interface moved parallel and radially from the centre to the wall of the TES. In Case 2 the interface assumed a kind of parabolic shape, while in Case 3 various cells with liquid PCM formed during the process.

As expected, the triplex heat exchanger (Cases 2 and 3) were the solutions that allowed the faster response of the TES device during the charge and discharge processes. The insertion of fins (Case 3) allowed, in particular, not only an increase in the heat exchange surface of the inner HTF tube, but also the creation of cells in the PCM volume that determined faster melting/solidification of the PCM.

A time of 12 and 8 hours was considered as a reference period for charge and discharge respectively. In this period, complete melting and solidification of the PCM was achieved only in Cases 2 and 3. A melted fraction for both phases was analyzed. A value of 1 for the charge process (complete melting) was achieved in about 9-10 hours in Cases 2 and 3, while a value of about 0.80-0,84 was reached in Case 1 in the same time interval. For the discharge process, a value of 0 (complete solidification) was achieved in about 4 hours in Cases 2-3, while a value of about 0.40 was reached in Case 1. The numerical result obtained in this work will be validated with experimental studies to be carried out in the experimental facility under test at the DIMCM.

4. References

[1] Adine H A and El Qarnia H 2009 Numerical analysis of the thermal behaviour of a shell-and-tube heat storage unit using phase change materials *Appl. Math. Model.* **33** 2132–44

[2] Akgün M, Aydin O and Kaygusuz K 2007 Experimental study on melting/solidification characteristics of a paraffin as PCM *Energy Convers. Manag.* **48** 669–78

[3] Gil A, Oró E, Miró L, Peiró G, Ruiz Á, Salmerón J M and Cabeza L F 2014 Experimental analysis of hydroquinone used as phase change material (PCM) to be applied in solar cooling refrigeration *Int. J. Refrig.* **39** 95–103

[4] Gil A, Medrano M, Martorell I, Lázaro A, Dolado P, Zalba B and Cabeza L F 2010 State of the art on high temperature thermal energy storage for power generation. Part 1-Concepts, materials and modellization *Renew. Sustain. Energy Rev.* **14** 31–55

[5] Gil A, Oró E, Peiró G, Álvarez S and Cabeza L F 2013 Material selection and testing for thermal energy storage in solar cooling *Renew. Energy* **57** 366–71

[6] Gil A, Barreneche C, Moreno P, Solé C, Inés Fernández a. and Cabeza L F 2013 Thermal behaviour of d-mannitol when used as PCM: Comparison of results obtained by DSC and in a thermal energy storage unit at pilot plant scale *Appl. Energy* **111** 1107–13

[7] Gil A, Oró E, Castell A and Cabeza L F 2013 Experimental analysis of the effectiveness of a high temperature thermal storage tank for solar cooling applications *Appl. Therm. Eng.* **54** 521–7

[8] Solé A, Neumann H, Niedermaier S, Martorell I, Schossig P and Cabeza L F 2014 Stability of sugar alcohols as PCM for thermal energy storage *Sol. Energy Mater. Sol. Cells* **126** 125–34
[9] Medrano M, Gil A, Martorell I, Potau X and Cabeza L F 2010 State of the art on high-temperature thermal energy storage for power generation. Part 2—Case studies *Renew. Sustain. Energy Rev.* **14** 56–72
[10] Choi J C and Kim S D 1992 Heat-transfer characteristics of a latent heat storage system using MgCl2 · 6H2O *Energy* **17** 1153–64
[11] Castell A, Solé C, Medrano M, Roca J, Cabeza L F and García D 2008 Natural convection heat transfer coefficients in phase change material (PCM) modules with external vertical fins *Appl. Therm. Eng.* **28** 1676–86
[12] Velraj R, Seeniraj R V., Hafner B, Faber C and Schwarzer K 1997 Experimental analysis and numerical modelling of inward solidification on a finned vertical tube for a latent heat storage unit *Sol. Energy* **60** 281–90
[13] Mehling H, Hiebler S and Ziegler F 2000 Latent Heat Storage using a PCM-graphite Composite Material *Terrastock 2000, 8th Int. Conf. Therm. Energy Storage* 375–80
[14] Agyenim F, Eames P and Smyth M 2009 A comparison of heat transfer enhancement in a medium temperature thermal energy storage heat exchanger using fins *Sol. Energy* **83** 1509–20
[15] Al-Abidi A a., Mat S, Sopian K, Sulaiman M Y and Mohammad A T 2013 Internal and external fin heat transfer enhancement technique for latent heat thermal energy storage in triplex tube heat exchangers *Appl. Therm. Eng.* **53** 147–56
[16] Mehling H and Cabeza L F 2008 2 Solid-liquid phase change materials *Heat cold storage with PCM. An up to date Introd. into basics Appl.*
[17] Sharma S D and Sagara K 2005 Latent Heat Storage Materials and Systems: A Review *Int. J. Green Energy* **2** 1–56
[18] Barreneche C, Gil A, Sheth F, Inés Fernández a. and Cabeza L F 2013 Effect of d-mannitol polymorphism in its thermal energy storage capacity when it is used as PCM *Sol. Energy* **94** 344–51
[19] Burger A, Henck J O, Hetz S, Rollinger J M, Weissnicht A a. and Stöttner H 2000 Energy/temperature diagram and compression behavior of the polymorphs of D-mannitol *J. Pharm. Sci.* **89** 457–68
[20] Bruni G, Berbenni V, Milanese C and Girella a 2009 Physico-chemical characterization of anhydrous D-mannitol *J. Therm. nalysis Calorimetrynalysis Calorim.* **95** 871–6
[21] Kumaresan G, Velraj R and Iniyan S 2011 Thermal Analysis of D-mannitol for Use as Phase Change Material for Latent Heat Storage *J. Appl. Sci.* **11** 3044–8
[22] Arena S, Cau G and Palomba C 2014 Development and implementation of a 3D numerical code for designing and predicting performances of PCM thermal energy storage systems *Eurotherm Semin. #99 Adv. Therm. Energy Storage* 1–9